SAND2007-1368C

# Monochromatic Soft X-Ray Self-Emission Imaging in Dense Z Pinches

B. Jones*, C. Deeney†, C. J. Meyer**, C. A. Coverdale*, P. D. LePell**, J. P. Apruzese‡, R. W. Clark‡ and J. Davis‡

*Sandia National Laboratories, PO Box 5800, Albuquerque, NM 87185 USA
†National Nuclear Security Administration, Washington, DC 20585 USA
** Ktech Corp., Albuquerque, NM 87123 USA
‡Naval Research Laboratory, Washington, DC 20375 USA

**Abstract.** The Z machine at Sandia National Laboratories drives 20 MA in 100 ns through a cylindrical array of fine wires which implodes due to the strong **j**x**B** force, generating up to 250 TW of soft x-ray radiation when the z-pinch plasma stagnates on axis. The copious broadband self-emission makes the dynamics of the implosion well suited to diagnosis with soft x-ray imaging and spectroscopy. A monochromatic self-emission imaging instrument has recently been developed on Z which reflects pinhole images from a multilayer mirror onto a 1-ns-gated microchannel plate detector. The multilayer provides narrowband (~10 eV) reflection in the 100-700 eV photon energy range, allowing observation of the soft emission from accreting mass as it assembles into a hot, dense plasma column on the array axis. Data at 277 eV photon energy have been obtained for plasmas ranging from Al to W, and the z-pinch implosion and stagnation will be discussed along with >1 keV self-emission imaging and spectroscopy. Collisional-radiative simulations are currently being pursued in order to link the imaged emissivity to plasma temperature and density profiles and address the role of opacity in interpreting the data.

**Keywords:** X-ray imaging, plasma diagnostics, wire array z pinch, multilayer mirror.
**PACS:** 52.58.Lq, 52.59.Qy, 52.70.-m, 52.70.La, 73.21.Ac

## INTRODUCTION

The Z machine [1] at Sandia National Laboratories is a pulsed power generator capable of driving a range of powerful, efficient z-pinch radiation sources for high-energy density physics experiments [2]. Compact tungsten wire arrays produce soft x-ray photons in the <1 keV range at powers >200 TW [3] for inertial confinement fusion research [4], while Al-Cu wire array and gas puff z pinches have been studied for generation of 1-8 keV K-shell radiation [5].

All classes of pinches studied on Z generate copious broadband radiation in the 100-1000 eV photon energy range, and thus time-resolved self-emission imaging through the use of a filtered pinhole camera is a standard diagnostic technique [6]. Filtered x-ray imaging can reject lower energy photons, providing a broadband higher photon energy image with a cutoff in the >1keV range. However, filtration alone cannot pass lower energy photons while rejecting higher energy x-rays in order to achieve narrowband monochromatic self-emission imaging. This can be accomplished by combining filtration with reflection from an x-ray mirror, and has

been studied using grazing incidence reflection from a Si mirror [7, 8] or from a multilayer mirror (MLM) [9] in z-pinch or laser-driven plasma experiments.

In this paper, we briefly describe an instrument employing MLM reflection for monochromatic imaging in the 100-700 eV range on the Z machine. This diagnostic has been described in greater detail in References [10-12]. In the following section, we describe the instrument and show an example of data from a Z wire array implosion. Then, future directions for quantitative analysis of the imaging data are discussed.

## DESCRIPTION OF THE X-RAY IMAGING DIAGNOSTIC

The Z MLM imager diagnostic combines a standard, filtered pinhole camera [Fig. 1(a)] with two pinhole cameras whose images are reflected from a MLM [one is shown in Fig. 1(b)]. Each MLM provides narrowband (~5 eV) reflection and serves as a monochromator. MLM reflectivity (R) and filter transmission (T) for a 277 eV photon imaging configuration that has been successfully fielded on Z are shown in Fig. 2. The calculation of this reflectivity curve and those for other untested configurations (Table I) are discussed in Ref. [12]. For each configuration, the designed MLM must be matched with a filter that can pass the MLM reflection under an absorption edge, but reject UV/visible reflection from the MLM and suppress second order reflection. The spatial resolution (Table I) is limited by diffraction for these low photon energies given the 3.56 m distance from source to pinholes [10] that is desired for ease of fielding outside the Z vacuum chamber and mitigation of debris damage of the device. As will be illustrated, however, the resolution is adequate for resolving the dynamics of the several-mm-scale imploding z pinches. Each camera employs eight pinholes and an eight-frame microchannel-plate detector for multi-point time-resolved (<1 ns) imaging [10].

Figure 3 shows imaging data collected over two nominally identical Z shots in which 60 mm on 30 mm diameter nested copper wire arrays were employed to

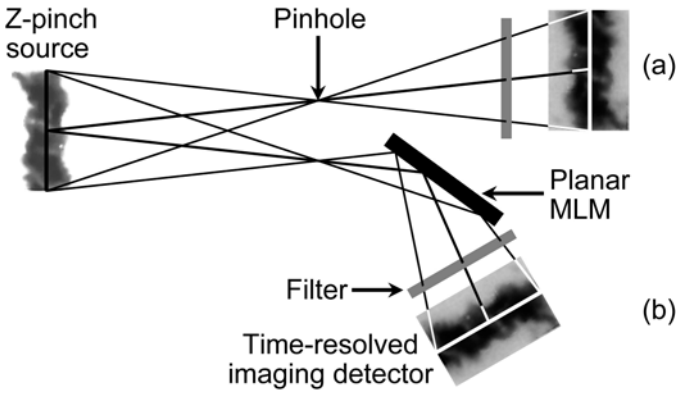


**FIGURE 1.** Instrument combines (a) a standard pinhole camera with (b) a pinhole imager reflecting from a multilayer mirror (MLM) monochromator.. Reprinted with permission from B. Jones *et al*., "Monochromatic X-Ray Self-Emission Imaging of Imploding Wire Array Z-Pinches on the Z Accelerator," IEEE T. Plasma Sci. **34**, 213 (2006), Fig. 1. ©2006, IEEE.

generate ~8 keV Cu K-shell [13]. These false-color, intensity-rescaled images display K-shell self-emission (standard pinhole configuration with 5 mils Kapton filter) in green, overlayed with 277 eV monochromatic emission in red; yellow indicates the superposition of both photon energies. The harder K-shell emission is seen to originate only from a narrow column on the wire array axis from early in time through the main x-ray power peak. In contrast, the 277 eV MLM-reflected images allow the observation of the cooler plasma that is accreting (and depositing energy) on axis over the rise of the main x-ray pulse. The radial distribution of the imploding mass is impacted by magnetic Rayleigh-Taylor instabilities growing from the start of the implosion [14], and the distribution of mass and its arrival time on axis is believed to determine the rise time of the x-ray pulse [4, 11]. Detailed study of the implosion kinetic energy, plasma energy deposition, and x-ray generation is ongoing.

The images in Fig. 3 also show a premature pinching of the plasma within 4 mm of the cathode, which is the glowing surface viewed at 12° from the horizontal at the bottom of each image. Strategies to mitigate this electrode effect are presently being

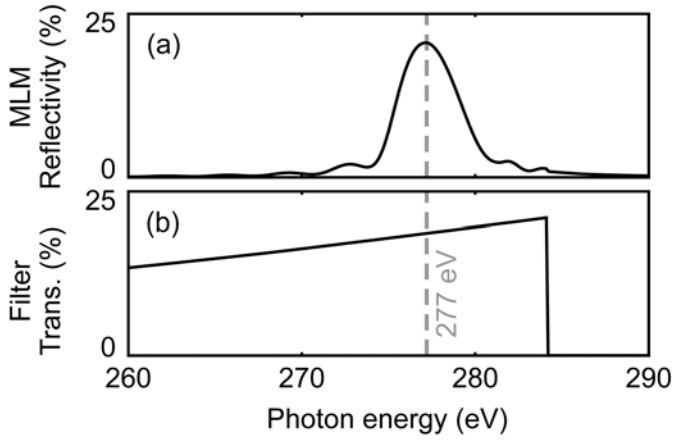


**FIGURE 2.** (a) Calculated reflectivity of the Cr/C MLM employed in the instrument (~40 Å period,~34° grazing angle). (b) 4-μm parylene-N+1000 Å Al filter passes the mirror reflection but suppresses visible light and second order reflection. Reprinted with permission from B. Jones *et al*., "Monochromatic X-Ray Self-Emission Imaging of Imploding Wire Array Z-Pinches on the Z Accelerator," IEEE T. Plasma Sci. **34**, 213 (2006), Fig. 2. ©2006, IEEE.

**TABLE 1. Proposed MLM/filter configurations for monochromatic imaging at various photon energies. These involve a simple swap of the Config. 2 filter and 34° grazing incidence MLM that is presently fielded on the Z machine.**

| Config. | Photon Energy (eV) | FWHM (eV) | Peak R (%) | Multilayer Materials | Bi-layer Period (Å) | Filter | Spatial Resolution (μm) |
|---|---|---|---|---|---|---|---|
| 1 | 96.2 | 8.3 | 59.9 | Mo/Si | 125 | 2.5 μm Be | 835 |
| 2 | 277.6 | 4.2 | 24.1 | Cr/C | 40.42 | 4 μm Parylene-N + 1000 Å Al | 482 |
| 3 | 442.1 | 5.4 | 4.1 | W/Si | 25.35 | 1 μm Ti | 382 |
| 4 | 500.0 | 5.0 | 4.9 | W/Si | 22.375 | 1 μm V | 359 |
| 5 | 527.6 | 3.9 | 5.1 | W/Si | 21.18 | 1 μm Cr | 350 |
| 6 | 700.0 | 4.3 | 4.2 | W/Si | 15.935 | 1 μm Fe | 304 |
| 7 | 768.7 | 3.0 | 4.4 | W/Si | 14.5 | 1 μm Ni | 290 |

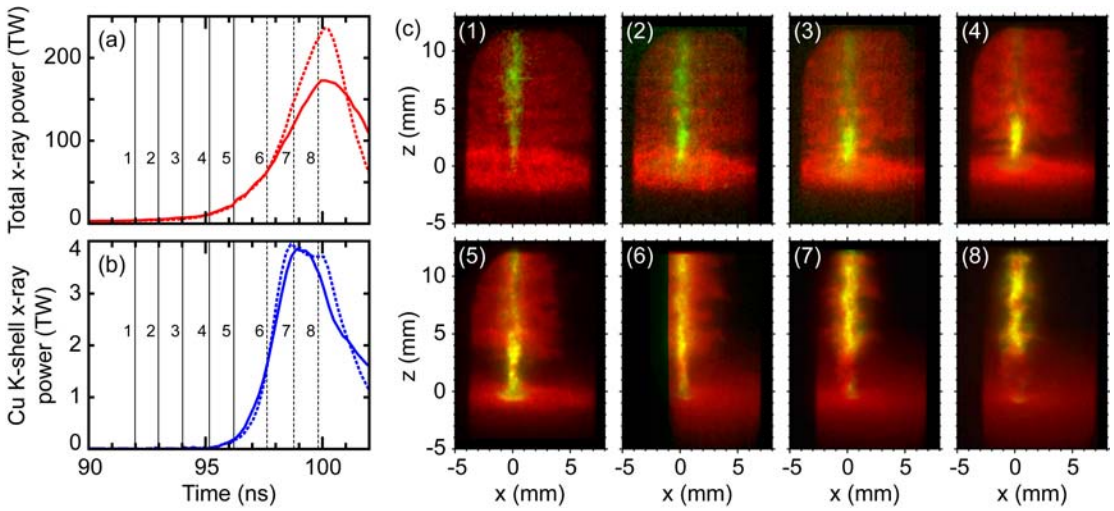


**FIGURE 3.** (a) Total radiated x-ray power and (b) ~8 keV Cu K-shell x-ray power with associated imager frame timing indicated for Z shots 1616 (dashed lines) and 1617 (solid lines). (c) False-color overlay of 277 eV (red) and Cu K-shell (green) self-emission images. Yellow indicates both 277 eV and K-shell emission superimposed. MLM-reflected images track the implosion of cooler trailing mass, which accretes on axis where K-shell emission is excited.

studied [15].

In addition to allowing observation of the cooler trailing mass, the 34°-grazing-angle MLM reflection also allows the detector to be shielded from direct line of sight from the x-ray source [10]. Background exposure of the detector caused by bremsstrahlung emission has been problematic with standard filtered pinhole cameras, but these hard photons pass are not reflected from the x-ray mirror and thus do not reach the detector, resulting in significant improvements in signal-to-noise in imaging configurations featuring mirror reflection [8, 11].

## COLLISIONAL-RADIATIVE SIMULATION AND FUTURE DIRECTIONS FOR DATA ANALYSIS

Images as shown in Fig. 3 paint a valuable qualitative picture of z-pinch dynamics, but we also wish to process the data to extract quantitative information. The diameter of the radiating, stagnated column can be measured in a straightforward manner, and is a necessary quantity for relating plasma properties to radiated power [16]. Furthermore, Abel inversion of the images has been pursued in order to track the evolution of the radial profile of plasma emissivity at 277 eV photon energy [11]. Emissivity profiles can be useful in benchmarking magnetohydrodynamic (MHD) simulations of the z-pinch implosion, but the monochromatic nature of the imaging data lends itself to further analysis in order to link emissivity with plasma density and temperature. We must also address whether opacity plays a role at the photon energy being imaged in order to justify Abel inversion, which implicitly assumes optically thin emission in most algorithms.

In this section, we discuss an example of analysis that begins to address these issues for a wire array z pinch plasma of alloy Al 5056 (95% Al, 5% Mg). This material was

chosen for this discussion as it is the lowest atomic number (and thus has the fewest atomic levels) of interest as a K-shell wire array radiator. Non-LTE collisional-radiative simulation was performed for such a plasma with the PrismSPECT code [17] which included all ground state levels, and all available Al and Mg levels for B-like through H-like charge states (4194 levels). This model is expected to be adequate for the range of plasma conditions of interest in imploding fast z pinches, except for electron temperature ($T_e$) less than 100 eV where C-like states are significantly populated in the code. This model could be further refined for accuracy in this region, and to speed calculation by judicious elimination or consolidation of atomic levels. The model incorporates radiation transport across a one-dimensional slab (1 mm path length is used, as relevant length scales in z pinches are of this order) in order to estimate opacity versus photon energy.

The strategy pursued here is to use estimates of emissivity ($\varepsilon$) and opacity ($\kappa$) versus photon energy from the atomic modeling along with MLM reflectivity (R) and filter transmission (T) for a given imaging configuration in order to estimate measured signal and optical depth and relate these to $T_e$ and plasma ion density $n_i$. Figure 4(a) shows R and T for configurations 2 and 6 of Table I; the product RT gives the instrument response versus photon energy. An example of modeled emissivity [Fig. 4(b)] and optical depth [Fig. 4(c)] over 1 mm path length are shown for plasma conditions of $T_e$=316 eV, $n_i=10^{19}$ cm$^{-3}$. The effective optical depth, indicated for the two imager configurations, is calculated using an effective opacity $\kappa_{eff} = \int_0^\infty RT\varepsilon dE \Big/ \int_0^\infty RT\varepsilon/\kappa dE$, integrated over photon energy $E=h\nu$ similarly to a Rosseland mean opacity but weighted also by instrument response. The quantity $\int_0^\infty RT\varepsilon dE$ is proportional to the quasi-monochromatic emissivity that is recovered from imaging data after Abel inversion.

Collisional-radiative simulations were carried out for a range of $T_e$, $n_i$ with the

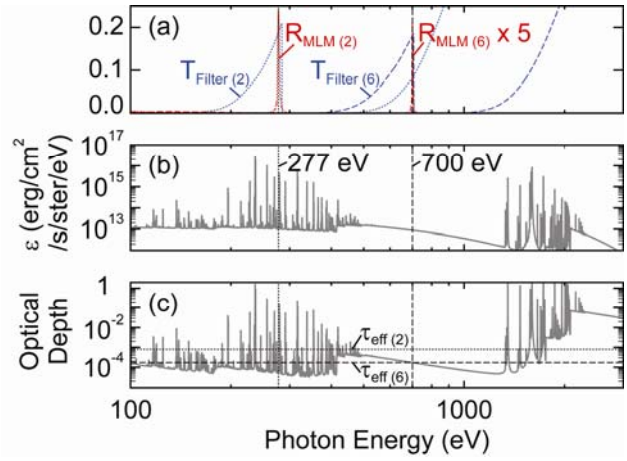


**FIGURE 4.** (a) MLM reflectivity (R) and filter transmission (T) versus photon energy for the imaging configurations 2 and 6 from Table I. (b) PrismSPECT modeled emissivity for $T_e$=316 eV, $n_i=10^{19}$ cm$^{-3}$, with config. 2 and 6 imaging energies indicated. (c) Modeled optical depth through 1 mm path length, with the effective optical depth ($\tau_{eff}$) of each imager configuration indicated by dashed horizontal lines.

quantity $\int_0^\infty RT\varepsilon dE$ representative of the measured signal shown in Fig. 5 (a) and (b) for imager configuration 2 and 6 respectively. The effective optical depth is shown versus $T_e$, $n_i$ in Fig. 5(c,d). As noted earlier, these models should be reasonable for $T_e \geq 100$ eV, which is likely the case in the final implosion stage of Al 5056 wire arrays on Z based on the observation of Al and Mg K-shell line emission from large radius at that time (detailed analysis is in progress) and on MHD simulation [15].

The first observation from Fig. 5(c,d) is that the emission for both photon energies considered is robustly optically thin for $T_e \geq 100$ eV, justifying the Abel inversion of the measured images. The simulation includes only two points per decade in $T_e$, $n_i$ space, but this conclusion seems convincing nonetheless based on the extremely low values of $\tau_{eff}$ for all points with $T_e \geq 100$ eV.

The second goal in discussing Fig. 5 is to address the relationship between $T_e$, $n_i$ and $\varepsilon$ in order to identify how to extract density or temperature profile information from Abel-inverted emissivity profiles. If the contours in Fig. 5(a,b) were vertical lines with $\varepsilon \propto n_i^2$, for example, then we could simply reconstruct the density profile by taking the square-root of the reconstructed $\varepsilon(r)$ profile (in arbitrary units in the present diagnostic implementation) and normalizing to the total initial wire array mass. Figure 5(a,b) exhibits temperature dependence as well, however, with a more complicated dependence at 277 eV (the present configuration implemented on Z) due to the line structure at that photon energy as seen in Fig. 4(b). By implementing configuration 6 at 700 eV in the future, it might be possible to image in the Al L-shell continuum, where a simple $\varepsilon \propto n_i^2$ dependence is seen in Fig. 5(b) along with a weak temperature dependence. Temperature dependence might be corrected for using $T_e(r)$ inferred through K-shell spectroscopy using a time- and space-resolved crystal spectrometer [18] (as mentioned, Al is overdriven on Z and is seen to emit K-lines at large radius from early in time).

To address these same issues of opacity and the relation of emissivity to plasma

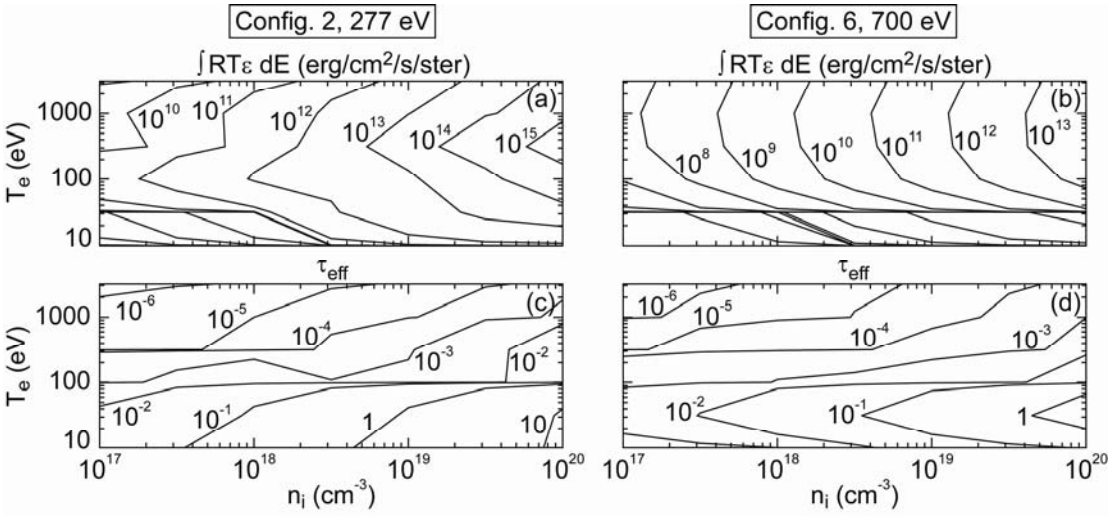


**FIGURE 5.** Representative measured signal (a, b) and effective optical depth (c, d) versus electron temperature and ion density for imager configurations 2 (a, c) and 6 (b, d), calculated using the PrismSPECT non-LTE collisional-radiative code.

conditions in higher-atomic-number-plasmas, the same techniques could be applied, though additional challenges would be presented by the increased atomic complexity. The number of levels included in the atomic physics models would likely need to be higher to capture the behavior of the emission spectrum with fidelity. Preliminary modeling for Cu indicates that the plasma is optically at 277 eV throughout the implosion [10], but adequacy of the L-shell model needs to be carefully considered. Another concern is that K-shell emission from Cu loads, for example, is seen only from on axis as discussed for Fig. 3. L-shell or even UV spectroscopy (which would also be more challenging due to the number of lines) might have to be explored for mid- to high-atomic-number elements in order to observe line emission from large radius early in time and have a hope of inferring the temperature profile.

Another approach might be profitable both for Al and higher-atomic-number plasmas—if monochromatic imaging could be obtained with absolute calibration at two nearby photon energies in the 100-1000 eV range, it might be possible to infer temperature profiles based on the ratio of the Abel-inverted emissivities. This has been previously suggested for monochromatic imaging of free-free continuum emission at higher x-ray photon energies ($E >> Z^2 \times 13.6$ eV) [19], and an analogous technique could be possible using either non-LTE collisional-radiative modeling or analytical theory in the Al L-shell continuum region, for example. The required absolute calibration could be obtained by normalizing each image to the power measured by an absolutely calibrated XUV diode viewing the z-pinch self-emission reflected from the same MLM (and passed by the same filter) that is used in the imaging instrument.

## SUMMARY

An x-ray self-emission imager has been fielded on Sandia's Z machine (a broadband source) that reflects pinhole images from a multilayer mirror in order to obtain monochromatic images with < 10 eV bandwidth in the 100-1000 eV range. Data has been successfully obtained at 277 eV photon energy from Al, Ar, stainless steel, Cu, and W z pinches. A similar instrument is being developed for the 8 MA Saturn generator; in addition to filtered K-shell and 277 eV monochromatic imaging, an imaging configuration at 528 eV corresponding to a prominent Ar L-shell line [12] will also be evaluated for imaging Ar gas puff z pinches. Time-resolved (1 ns), eight-frame microchannel plate detectors provide imaging at three separate energies (two monochromatic MLM-reflected, one filtered for broadband response) for both of these diagnostic instruments.

Monochromatic imaging through x-ray reflection provides several key advantages. The background exposure of the detector can be significantly reduced by shielding from hard x-rays, which do not reflect from the mirror. The use of a multilayer reflecting in the 100-1000 eV photon energy range allows the cooler trailing mass to be observed during the z-pinch implosion, while >1 keV filtered imaging preferentially sees the hot, dense mass accumulating on the z-pinch axis. Abel inversion of the monochromatic self-emission images allows dynamics of the implosion phase to be explored and compared to MHD code simulations.

Future work will pursue quantitative measurement of temperature and density profiles by relating measured emissivity to plasma conditions via non-LTE collisional-radiative simulation. Preliminary analysis indicates that the density profile can be inferred through the combined use of monochromatic self-emission imaging, Abel inversion to obtain $\varepsilon(r)$, $T_e(r)$ measured through K-shell spectroscopy (or two-color emissivity ratios), and collisional-radiative modeling to relate emissivity and plasma conditions. Additional imager configurations as in Table I will be tested on Z and Saturn, and wire array and gas puff z-pinch dynamics will be further investigated through this x-ray imaging technique.

## ACKNOWLEDGMENTS

The authors would like to thank G. Dunham (Ktech), L. P. Mix, K. Peterson, G. A. Rochau, J. E. Bailey (Sandia), and R. Mancini (University of Nevada, Reno) for helpful discussions and assistance with data analysis; D. Petmecky, P. Gard, and C. Ball (TMI, Inc.) for valuable contributions to the design and manufacture of the instrument; and T. C. Moore (Ktech), P. W. Lake, and N. R. Joseph (Sandia) for assistance in fielding the instrument on the Z machine. This work was supported by Sandia National Laboratories, a multiprogram laboratory operated by Sandia Corporation, a Lockheed Martin Company, for the United States Department of Energy's National Nuclear Security Administration under contract DE-AC04-94AL85000.

## REFERENCES

1. Spielman, R. B., *et al*., *Phys. Plasmas* **5**, 2105-2111 (1998).
2. Matzen, M. K., *Phys. Plasmas* **12**, 055503-1—055503-16 (2005).
3. Deeney, C., *et al*.., *Phys. Rev. Lett.* **81**, 4883-4886 (1998).
4. Cuneo, M. E., *et al*., *Phys. Plasmas* **13**, 056318-1—056318-18 (2006).
5. Jones, B., *et al*., *J. Quant. Spectrosc. Radiat. Transfer* **99**, 341-348 (2006).
6. Nash, T. J., *et al*., *Rev. Sci. Instrum.* **72**, 1167-1172 (2001).
7. Wenger, D. F., *et al*., *Rev. Sci. Instrum.* **75**, 3983-3985 (2004).
8. Nash, T. J., *et al*., *Rev. Sci. Instrum.* **77**, 10E319-1—10E319-4 (2006).
9. Koch, J. A., *et al*., *Rev. Sci. Instrum.* **76**, 073708-1—073708-4 (2005).
10. Jones, B., *et al*., *Rev. Sci. Instrum.* **75**, 4029-4032 (2004).
11. Jones, B., *et al*., *IEEE T. Plasma Sci.* **34**, 213-222 (2006).
12. Jones, B., *et al*., *Rev. Sci. Instrum.* **77**, 10E316-1—10E316-4 (2006).
13. Coverdale, C. A., *et al*., *IEEE T. Plasma Sci.*, submitted (2007).
14. Sinars, D. B., *et al*., *Phys. Plasmas* **12**, 056303-1—056303-8 (2005).
15. Jennings, C. A., private communication (2007).
16. Apruzese, J. P., *et al*., *J. Quant. Spectrosc. Radiat. Transfer* **57**, 41-61 (1997).
17. MacFarlane, J. J., *et al*., "Simulation of the ionization dynamics of aluminum irradiated by intense short-pulse lasers" in *International Conference on Inertial Fusion Sciences and Applications-2003*, edited by B. A. Hammel *et al*., La Grange Park, IL: American Nuclear Soc., 2004, pp. 457-460.
18. Bailey, J. E., *et al*., *Phys. Rev. Lett.* **92**, 085002-1—085002-4 (2004).
19. Koch, J.A., *et al*., *J. Quant. Spectrosc. Radiat. Transfer* **88**, 433-445 (2004).